

Enhancement of superconductivity by the small size effect in In nanoparticlesW.-H. Li,^{1,2,*} C. C. Yang,² F. C. Tsao,¹ S. Y. Wu,¹ P. J. Huang,¹ M. K. Chung,¹ and Y. D. Yao²¹*Department of Physics, National Central University, Chung-Li, 32001 Taiwan*²*Institute of Physics, Academia Sinica, Taipei, 115 Taiwan*

(Received 14 June 2005; revised manuscript received 12 September 2005; published 20 December 2005)

The superconducting parameters of zero-dimensional In nanoparticles were studied by measuring the magnetic susceptibility, electrical resistivity, and specific heat. Significant alternations of the superconducting parameters were found for particles with diameters smaller than 120 nm. The Anderson regime, where superconductivity was sharply suppressed by the discrete nature of the electronic levels, was seen for particle smaller than 7.5 nm. A regime prior to the Anderson one, in which superconductivity was found to vary in accordance with alternations of the structural parameters, due to the small size effect, was also observed and characterized. A nonignorable 5 % increase in T_C and a 400 times higher H_C were seen for the 39 nm particles. The appearance of this regime was closely related to the structural symmetry of the system.

DOI: [10.1103/PhysRevB.72.214516](https://doi.org/10.1103/PhysRevB.72.214516)

PACS number(s): 74.81.Bd, 73.63.Bd, 74.62.Bf, 81.07.Wx

Since the formulation of the microscopic BCS theory,¹ weakly coupled superconductivity, such as that observed in indium,² may be understood by the electron-phonon coupling. It is known that both the electron and lattice characteristics can be greatly modified when the size of the system is reduced to the nanometer scale, where the effects originated from the disruption of lattice periodicity at the particle surface, known as the small size effect, and from the appearance of discrete electron levels due to quantum confinement, may become significant. This means that the superconducting parameters of nanoparticles may be dramatically different from particles in the bulk form.³ Apparently, the most noticeable finite size effect is the loss of superconductivity, when the electron level separation near the Fermi level becomes comparable to the BCS superconducting gap.⁴ This criterion, known as the Anderson criterion, usually occurs when particles are a few nanometer in size,^{5,6} which is generally much smaller than when the small size effect has become nonignorable. The small size effect frequently results in lattice rearrangement and crystalline imperfections. Superconducting properties may consequently be altered as well. It appears that most of the experimental works on low-dimensional superconductivity have been performed on mesoscopic thin films. A critical thickness for the occurrence of superconductivity⁷ and an oscillating superconducting transition temperature T_C with the film thickness⁸ have both been observed in Pb films. Effects of film topology on the superconductivity have also been investigated in Al films,⁹ and size-dependent breakdown of superconductivity has been studied in Al nanowires.¹⁰ The connections between the suppression of superconductivity in nanowires and the occurrence of quantization localization, known as dissipative phase transition,¹¹ have been investigated using ultrathin $\text{Mo}_{79}\text{Ge}_{21}$ nanowires.¹² For zero-dimensional particles, microscopic tunneling experiments have been used to investigate the loss of superconductivity in small Al grains embedded in an insulating matrix,¹³ while magnetization measurements have been used for Pb nanoparticles.^{14,15} Superconductivity in Pt has recently been discovered, but only when it is prepared into small nanoparticles and at temperatures of a few millidegrees Kelvin.¹⁶ Until recently, studies

on the influences of the small size effect on superconductivity have been very limited. In this paper, we report on the effects of particle size on the superconductivity of tetragonal In nanoparticles. Before the particles were small enough to reach the Anderson regime, in which superconductivity is sharply suppressed as the particle size is deduced, a regime was also observed in which T_C increases noticeably before lattice strain builds up, which then gradually suppresses T_C . We attribute the appearance of this regime in tetragonal In nanoparticles to the occurrence of lattice instability caused by the small size effect. No similar regime was found in cubic Pb nanoparticles.

A series of ten sets of In nanoparticle powders were fabricated by employing the gas condensation method. High-purity indium ingots were evaporated in an Ar atmosphere (0.02–1 torr), using an evaporation rate of 0.05 Å/s. A stainless-steel plate, maintained at the liquid-nitrogen temperature, was used to collect the evaporated particles. After restoration to room temperature, the nanoparticles, which were only loosely attached to the collector, were stripped off. These assemblies of macroscopic amounts of individual In nanoparticles were in powdered forms. The samples were, slightly but not extremely, sensitive to being exposed to air. However, they were still kept in a vacuum at all times to avoid possible surface oxidization.

High-resolution x-ray diffraction, atomic-force microscopy (AFM), and transmission electron microscopy (TEM) were used to determine the mean particle diameters and size distributions of the powders. All the diffraction peaks can be associated with a tetragonal body-centered In structure. No oxidation phases, such as InO and In_2O_3 , were found to within the 3 % x-ray resolution limitation. The diffraction peaks appeared much broader than those of the instrumental resolutions, reflecting the finite-size effect. A representative {101} diffraction profile for the body-centered structure is shown in Fig. 1, where the observed (open circles), fitted (solid curve), and instrumental resolution (dotted curve) profiles for the 10.5 nm particles are displayed. Size analyses based on the AFM and TEM images show that the size distribution can be described using a Gaussian function. Par-

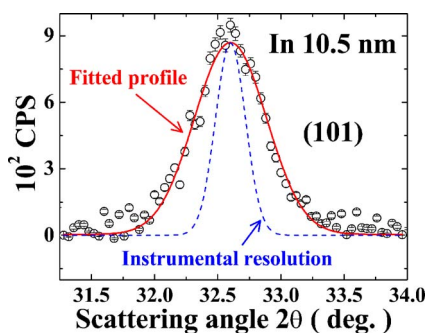


FIG. 1. (Color online) Plots of the observed (open circles), the fitted (solid curve), and the instrumental resolution (dotted curve) profiles of the characteristic $\{101\}$ x-ray reflection for a body-centered structure, obtained at room temperature on a representative In nanoparticle powder. Line broadening, resulting from the finite size effect, can be clearly seen in the diffraction peak. A mean particle diameter of 10.5(5) nm was obtained for the sample.

ticles smaller than and larger than 20 nm have typically half-widths of 2 and 4 nm, respectively. A portion of a TEM image and the corresponding size distribution, obtained from a $0.4 \times 0.5 \mu\text{m}^2$ image, are shown in Fig. 2. This image was obtained by very loosely spreading the nanoparticles onto a copper grid and was taken on a JEOL2000FX transmission electron microscope, employing an accelerating voltage of 160 kV. A quite symmetrical size distribution was obtained, which could be described using a Gaussian function (shown as the solid curve on the data), with its center at 7.5 nm and a half-width of 1.8 nm. We determine the mean particle diameters d by fitting the diffraction patterns (solid curve shown in Fig. 1) to the diffraction profiles of finite-sized particles, assuming the same size distribution as that obtained from the AFM and TEM images. The mean particle diameters determined for the ten sets of samples ranged from 3.0(4) to 120(5) nm. Table I lists the fabrication conditions and corresponding mean particle diameters of the resultant nanoparticle powders in the series studied. It appears that smaller particles were obtained when a higher chamber pressure was used, which also required a higher heating current. All In nanoparticles studied retained the same tetragonal body-centered structure, as in bulk In.^{17,18} Nevertheless, noticeable alternations in lattice parameters a and c were seen for particles with diameters smaller than ~ 120 nm. Figure 3 shows the size dependencies of c/a , the cell volume, and the lattice strain, obtained from Rietveld refining¹⁹ the x-ray-diffraction patterns. It clearly reveals that c/a decreases upon

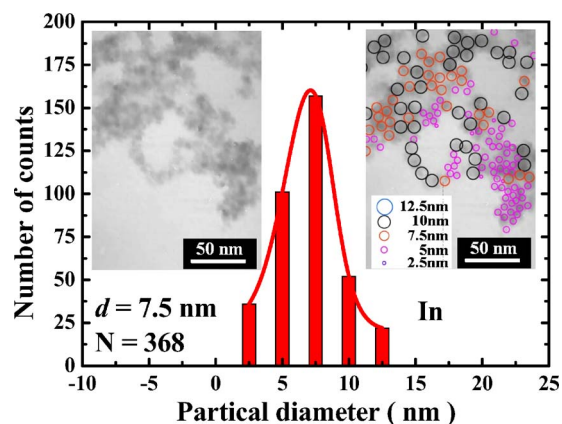


FIG. 2. (Color online) A portion of a TEM image and the size distribution obtained from the image. The circles shown on the image indicate the scales used in obtaining the size distribution. A symmetrical size distribution is obtained that may be described by using a Gaussian distribution function, with a center at 7.5 nm and half-width of 1.8 nm, indicated by the solid curve.

reducing d , reaching a minimum at $d \sim 30$ nm. Below that, c/a increases upon further reduction of d , as the lattice strain begins to build up and the unit cell expands. We note that the cell volume remains unchanged until the lattice strain becomes significant. These observations of cell parameter variations are different from those that have been observed¹⁸ for bulk In under pressure. The small size effect, originating from the disruption of the lattice periodicity, is likely the main mechanism behind the present observations.

The dc electrical resistivity, ac magnetic susceptibility, and specific heat were all measured to explore the superconducting properties of the nanoparticles. Specific heat data were taken by employing the thermal relaxation method, whereas resistivity measurements were performed using the standard four-probe setup. For the resistivity measurements, the nanoparticles were densely packed into a small insulating cell ($\sim 3 \times 2 \times 1 \text{ mm}^3$), with a mass density of $\sim 67\%$ that of bulk In, to reduce resistance from the interparticle spatial gaps. The nanoparticles were then weakly linked, with an average interparticle spatial gap of ~ 0.5 nm. Finite resistances at low temperatures, from the interparticle spatial separation, can then be anticipated. On the other hand, to reduce the coupling that may arise among the nanoparticles, the magnetic susceptibility measurements were performed using very loosely packed nanoparticle powders, with a mass density of $\sim 0.8\%$ that of bulk In, which corresponds to an average interparticle spatial gap of ~ 36 nm.

TABLE I. List of the fabrication conditions and the mean particle diameters of the resultant In nanoparticles, where P , I , d , and T_C represent the evaporation Ar pressure, applied heating current, mean particle diameter, and superconducting transition temperature, respectively.

	Evaporation rate=0.05 Å/s, Distance between collector and source=14 cm.									
P (torr)	1.0	0.85	0.7	0.6	0.5	0.35	0.1	0.1	0.05	0.02
I (amp)	150	150	130	130	125	125	120	120	120	120
d (nm)	3	5	6.5	7.5	10.5	20	36	39	87	120
T_C (K)	<1.4	<1.4	2.24	3.36	3.51	3.55	3.53	3.58	3.5	3.4

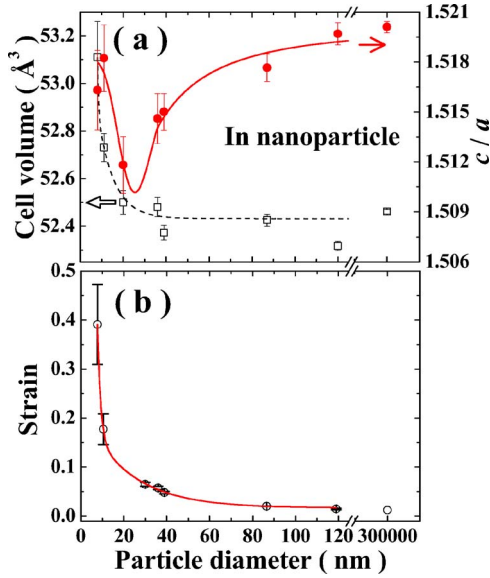


FIG. 3. (Color online) Plots of the variations of the lattice parameter ratio c/a , the cell volume, and the lattice strain with the particle diameter for In nanoparticles. It is clear that c/a begins to decrease when particles are smaller than ~ 120 nm, reaching a minimum at $d \sim 30$ nm, smaller than which, c/a begins to increase as the lattice strain begins to build up and the unit cell expands.

Figure 4 shows the temperature dependencies of the resistivity ρ , the in-phase component of the magnetic susceptibility χ' , and the specific heat C of the representative 10.5 nm particles. All three curves display anomalous changes at 3.5 K, signaling the occurrence of superconductivity. It appears that the transition occurred over a broad temperature range, indicating that the spatial fluctuations of the superconducting order parameters had become significant, which was a result of the limitations of the superconducting characteristic lengths related to the particle size.²⁰ We note that finite resistivity at ~ 0.8 m Ω cm was obtained at low temperatures, indicating that it does not lead to a global superconducting state in the nanoparticle compact used for the resistivity measurements. The samples used for the resistivity measurements consist of weakly linked nanoparticles, with an average interparticle separation of ~ 0.5 nm, where electron transport certainly engaged interparticle tunneling and Josephson junctions may form when nanoparticles become superconducting. It appears that Josephson supercurrent was not allowed through the whole sample. The finite resistivity observed at low temperatures may then simply account for the resistivity of the interparticle links and the drop signals the reduction in resistivity as the nanoparticles become superconducting. We estimated that the appeared resistivity for each interparticle tunneling was ~ 4 n Ω cm. Furthermore, a kink at ~ 2.5 K appears in the $\rho(T)$ curve as well. The origin of this behavior is not completely understood to us at the present time. This kink, however, seems to echo the appearance of the low-temperature peak in $C(T)$. We attribute these anomalies to be associated with the discrete nature of the electronic levels in nanoparticles. On warming, a reduction in the increase rate of resistivity can be anticipated, once the thermal energy becomes comparable with the level separation.

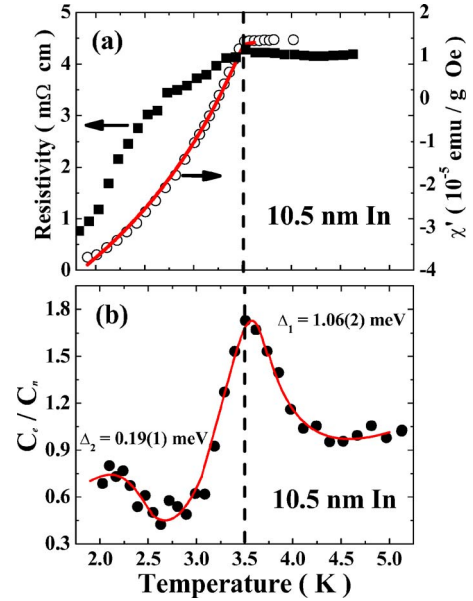


FIG. 4. (Color online) Plots of the temperature dependencies of (a) the electrical resistivity and magnetic susceptibility, and (b) the specific heat of the 10.5 nm In nanoparticles. All three curves display anomalous changes at 3.5 K, signaling the occurrence of superconductivity.

The $\chi'(T)$ shown in Fig. 4(a) may be described using Scalapino's expression,^{21,22} where the effects originating from the penetration of the field into the particle, from the discreteness in the spectrum, and from the temporal fluctuations of the order parameters, have all been accounted for. For spherical particles of diameter d and mass density σ , the diamagnetic susceptibility can be written as²³

$$\chi'_{\text{dia}} = -\frac{1}{4\pi} \left\{ \frac{3}{2\sigma} \left[1 - \frac{6\lambda_L}{d} \text{Coth}\left(\frac{d}{2\lambda_L}\right) + \frac{12\lambda_L^2}{d^2} \right] \right\},$$

where the penetration depth λ_L varies with temperature according to²²

$$\lambda_L(T) = \frac{\lambda_{L0}}{\sqrt{\frac{1}{\pi} \left(\frac{\delta}{b}\right)^{1/2} \left(\frac{2}{\sqrt{\pi}} \frac{\exp(-\theta^2)}{1 \pm \text{Erf}(|\theta|)} - 2\theta \right)}},$$

λ_{L0} is the penetration depth at zero temperature, $\delta \equiv \Delta/k_B T_C$, k_B is the Boltzmann's constant, Δ is the single electron level spacing, $b \equiv 7\zeta(3)/16 = 0.526$, $\zeta(3)$ is the Riemann zeta function of order 3, Erf stands for the error function, $\theta \equiv \frac{1}{2}\pi(t-1)/(b\delta)^{1/2}$, $t \equiv T/T_C$ is the reduced temperature, and the upper and lower signs of \pm in the above expression applied for θ is negative and positive, respectively. The solid curve shown on the $\chi'(T)$ in Fig. 4(a) is the result of fits of the data to $\chi' = \chi'_{\text{dia}} + \chi'_0$, where χ'_0 accounts for the Pauli magnetic susceptibility, with fitted values of $T_C = 3.51(3)$ K and $\lambda_{L0} = 2.8(4)$ nm for the 10.5 nm particles.

Two distinct peaks at around 3.5 and 2.1 K can be seen in the normalized specific heat curve shown in Fig. 4(b), where the βT^3 contributions from phonons have been subtracted from the data. These calorimetric data may be described

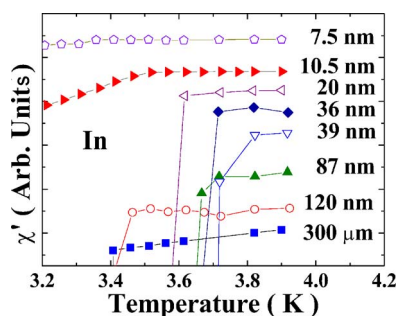


FIG. 5. (Color online) Plots of $\chi'(T)$ near the superconducting transition regime for several of the In nanoparticles. It is clear that the temperature at which the diamagnetic screening signal appears shifts consistently to a higher temperature as the size is reduced, reaching 3.7 K for the 39 nm particles, smaller than which it decreases as the size is reduced further.

(solid curve) using Scalapino's expression,²² with the appearance of two energy gaps of $\Delta_1=1.06(2)$ meV and $\Delta_2=0.19(1)$ meV. The appearance of Δ_1 reflects the occurrence of superconductivity, whereas Δ_2 is associated with the emergence of the discrete electron levels anticipated for finite size particles. The fitted value of $\Delta_1=1.06$ meV agrees well with the superconducting gap of 1.05 meV for bulk In, and $\Delta_2=0.19$ meV fits the average level spacing of 0.17 meV for 10.5 nm In particles well, as estimated according to the Kubo formula.^{3,24}

Superconductivity was observed for all but the 3 and 5 nm particles, for which monotonic increases in χ' and ρ , upon cooling to 1.4 K, were seen. We note that for In the critical particle diameter for supporting BCS superconductivity, estimated according to Smith and Ambegaokar⁶ and Kubo²⁴ formulas, is 5.9 nm. This agrees with the present observations. For particles with diameters smaller than 120 nm, the superconducting parameters were found to be greatly affected by the particle size. A representative plot, reflecting the effects of finite size on T_C , is shown in Fig. 5, where $\chi'(T)$ near the transition regimes in several samples are plotted together for a direct comparison. It can clearly be seen that the temperature at which diamagnetic screening signals appear shifts consistently to a higher temperature, with a reduction in particle size, until reaching 3.7 K for the 39 nm particles, below which, it shifts to lower temperatures as the size is reduced further. No obvious change in T_C was found for particles larger than 120 nm, hence the bulk regime. At the other extreme, the Anderson regime lies between 7.5 and 5 nm, as T_C of the 7.5 nm particles appears at 3.36 K, that of the 6.5 nm particles at 2.24 K, and that of the 5 nm particles at below 1.4 K, if it does superconduct. It hence displays a sharp drop in the $T_C(d)$ curve for this regime. Our previous studies¹⁵ showed that the Anderson regime for Pb lies between 9 and 3 nm. It is known that Anderson regime depends on the relation between the superconducting gap and the electronic level spacing. A lower electron density gives rise to a larger average level spacing in a fixed particle size,^{3,20} while the BCS superconductivity may be anticipated to breakdown when the level spacing reaches 0.89 and 4×0.89 times of the superconducting gap for particles with odd and even number of electrons,

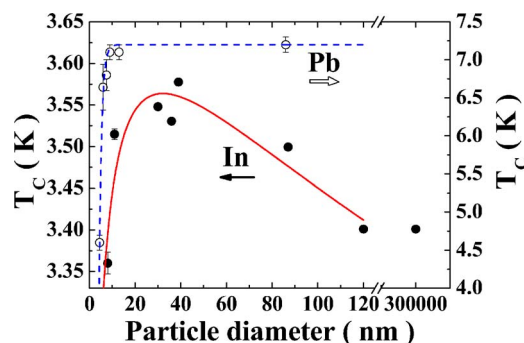


FIG. 6. (Color online) Plots of the variations of T_C with particle size for In (filled symbols) and Pb (open symbols) nanoparticles. A peak structure is seen in the $T_C(d)$ plot of In, whereas that of Pb displays a monotonic and sharp crossover from the bulk to the Anderson regimes.

respectively.^{5,6} The relatively narrow Anderson regime observed for In is then a result of the combinations of a small superconducting gap, a low density of electronic states at the Fermi surface, and having an odd number of electrons for In.

The size dependence of T_C in the intermediate regime, obtained from the fits of the $\chi'(T)$ data to the Scalapino's expression,^{21,22} is plotted (filled symbols) in Fig. 6. There is a peak structure in the $T_C(d)$ plot and the T_C for the 39 nm particles reaches 3.58 K, a nonignorable 5 % increase, compared to the T_C of bulk In. Similar peak structures can also be seen in the critical magnetic field versus particle-size plot and in the coupling strength versus particle-size plot. Note that H_C of the 39 nm particles increases to 116 KOe, which is a factor of ~ 400 times higher than that of bulk In. Surface superconductivity may not be the main mechanism accounting for the present observation of enhanced superconductivity, since it is difficult to distinguish surface from inner superconductivity when particle sizes are much smaller than the superconducting length scales. Note that the London penetration depth and coherence length of bulk In are 64 and 364 nm, respectively. The regime for d is smaller than ~ 30 nm, where T_C was found to be decreased when d is reduced. This regime may not be a portion of the Anderson regime, since the reduction rate for these two portions differs by a factor of ~ 120 and an insignificant level spacing of $7 \mu\text{eV}$ is expected for 30 nm In particles, when estimated according to the Kubo formula. Interestingly, this is the same regime where obvious alternations in the structural parameters were observed. The $T_C(d)$ curve echoes the $a/c(d)$ curve shown in Fig. 3. This strongly suggests that the variations of T_C in this regime are closely related to the alternations of the structural parameters caused by the small size effect. The enhancement of the superconductivity originates from the decrease of the lattice parameter ratio c/a . Once the lattice strain builds up, the unit cell expands, c/a relaxes, and superconductivity weakens.

No similar behaviors, of T_C being noticeably affected by the small size effect, were observed in Pb nanoparticles,¹⁵ where $T_C(d)$ displays a monotonic and sharp crossover from the bulk to the Anderson regimes, as shown (open symbols) in Fig. 6, and in Pb granular films.²⁵ These differences mainly originated from the difference in the crystalline struc-

ture of the two elements. Indium crystallizes into a body-centered tetragonal structure with $c/a \sim 1.5$, whereas Pb enters a fcc one.^{17,18} The anisotropic and relatively loose packing of In atoms not only results in a much smaller density (50% smaller than that of Pb) and a much higher thermal expansion coefficient (10^4 times higher than that of Pb), but apparently also significantly responds to the small size effect by reducing c/a . The reduction of c/a , while the unit cell volume remains unchanged, may cause phonon softening, which increases the electron-phonon coupling²⁶ and enhances superconductivity. The enhancement of T_C in small superconducting particles has previously been observed²⁷ in granular Al films as well. Ginzburg has pointed out²⁸ that the enhancement of this kind can be connected to the softening of surface phonons. Our studies clearly show that in zero-dimensional In nanoparticles it is the structural change that triggers the enhancement.

In conclusion, a superconducting phase associated with the variations in the lattice parameters, caused by the small size effect, has been observed in zero-dimensional tetragonal In nanoparticles. This superconducting regime appears before the particles are small enough to enter the Anderson regime. For indium, the Anderson regime covers a very narrow range in terms of particle size, due to the small superconducting gap and low density of the electronic states. Detailed mapping of the $T_C(d)$ curve of the Anderson regime for zero-dimensional In nanoparticles is then very difficult. Finally, we remark that the appearance of the newly observed superconducting phase, prior to the Anderson one, is closely related to the structural nature of the system.

This work was supported by the National Science Council of the Republic of China under Grant No. NSC-94-2120-M-008-003.

*Corresponding author. Email address: whli@phy.ncu.edu.tw

- ¹J. Bardeen, L. N. Cooper, and J. R. Schrieffer, *Phys. Rev.* **108**, 1175 (1957).
- ²*A Physicist's Desk Reference*, 2nd ed., edited by H. L. Anderson, (American Institute of Physics, New York, 1989), p. 117.
- ³See, for example, W. P. Halperin, *Rev. Mod. Phys.* **58**, 533 (1986).
- ⁴P. W. Anderson, *J. Phys. Chem. Solids* **11**, 28 (1959).
- ⁵J. von Delft, A. D. Zaikin, D. S. Golubev, and W. Tichy, *Phys. Rev. Lett.* **77**, 3189 (1996).
- ⁶R. A. Smith and V. Ambegaokar, *Phys. Rev. Lett.* **77**, 4962 (1996).
- ⁷K. L. Ekinci and J. M. Valles, Jr, *Phys. Rev. Lett.* **82**, 1518 (1999).
- ⁸Y. Guo, Y. F. Zhang, X.-Y. Bao, T.-Z. Han, Z. Tang, L.-X. Zhang, W.-G. Zhu, E. G. Wang, Q. Niu, Z. Q. Qiu, J.-F. Jia, Z.-X. Zhao, and Q.-K. Xue, *Science* **306**, 1915 (2004).
- ⁹V. V. Moshchalkov, L. Gielen, C. Strunk, R. Jonckheere, X. Qiu, C. Van Haesendonck, and Y. Bruynseraede, *Nature (London)* **373**, 319 (1995).
- ¹⁰M. Zgirski, K.-P. Riihonen, V. Touboltsev, and K. Arutyunov, *Nano Lett.* **6**, 1029 (2005).
- ¹¹J. S. Penttila, U. Parts, P. J. Hakonen, M. A. Paalanen, and E. B. Sonin, *Phys. Rev. Lett.* **82**, 1004 (1999).
- ¹²A. Bezryadin, C. N. Lau, and M. Tinkham, *Nature (London)* **404**, 971 (2000).
- ¹³C. T. Black, D. C. Ralph, and M. Tinkham, *Phys. Rev. Lett.* **76**,

688 (1996); D. C. Ralph, C. T. Black, and M. Tinkham, *ibid.* **78**, 4087 (1997).

- ¹⁴S. Reich, G. Leitner, R. Popovitz-Biro, and M. Schechter, *Phys. Rev. Lett.* **91**, 147001 (2003).
- ¹⁵W.-H. Li, C. C. Yang, F. C. Tsao, and K. C. Lee, *Phys. Rev. B* **68**, 184507 (2003).
- ¹⁶J. F. Annett, *Superconductivity, Superfluids and Condensates* (Oxford University Press, London, 2004), p. 50.
- ¹⁷C. Kittel, *Introduction to Solid State Physics*, 7th ed. (Wiley, New York, 1996), p. 23.
- ¹⁸A. S. Mikhaylushkin, U. Haussermann, B. Johansson, and S. I. Simak, *Phys. Rev. Lett.* **92**, 195501 (2004).
- ¹⁹H. M. Rietveld, *J. Appl. Crystallogr.* **2**, 65 (1969).
- ²⁰R. Kubo, A. Kawabata, and S. Kobayashi, *Annu. Rev. Mater. Sci.* **14**, 49 (1984).
- ²¹J. P. Hurault, K. Maki, and M. T. Beal-Monod, *Phys. Rev. B* **3**, 762 (1971).
- ²²B. Mühlischlegel, D. J. Scalapino, and R. Dento, *Phys. Rev. B* **6**, 1767 (1972).
- ²³D. Shoenberg, *Proc. R. Soc. London, Ser. A* **A175**, 49 (1940).
- ²⁴R. Kubo, *J. Phys. Soc. Jpn.* **17**, 975 (1962).
- ²⁵E. T. S. Appleyard, I. R. Bristow, H. London, and A. D. Misner, *Proc. R. Soc. London, Ser. A* **A172**, 540 (1939).
- ²⁶J. C. Phillips, *Physics of High- T_C Superconductors* (Academic Press, San Diego, 1989), Chap. 1.
- ²⁷R. W. Cohen and B. Abeles, *Phys. Rev.* **168**, 444 (1968).
- ²⁸V. L. Ginzburg, *Physica (Amsterdam)* **13**, 101 (1964).